

A Unified Strouhal-Reynolds Number Relationship for Laminar Vortex Streets Generated by Different Shaped Obstacles

Ildoo Kim*

School of Engineering, Brown University, Providence, RI 02906 and

Department of Physics and Astronomy,

University of Pittsburgh, Pittsburgh, PA 15260

X.L. Wu

Department of Physics and Astronomy,

University of Pittsburgh, Pittsburgh, PA 15260

(Dated: August 12, 2015)

Abstract

A new Strouhal-Reynolds number relationship, $St = 1/(A + B/Re)$, has been recently proposed based on observations of laminar vortex shedding from circular cylinders in a flowing soap film. Since the new $St-Re$ relation was derived from a general physical consideration, it raises the possibility that it may be applicable to vortex shedding from bodies other than circular ones. The work presented herein provides experimental evidence that this is the case. Our measurements also show that in the asymptotic limit ($Re \rightarrow \infty$), $St_\infty = 1/A \simeq 0.21$ is constant independent of rod shapes, leaving B the only parameter that is shape dependent.

* ildoo_kim@brown.edu

When a flowing fluid encounters an obstacle, two staggered rows of vortices form downstream. This so-called von Kármán vortex street has been studied by scientists for many years [1–5], but our basic understanding of vortex wake formation, its stability, and evolution remains incomplete. At the heart of the problem is why and how vorticity, which is created in the boundary layer and discharged into a bulk of fluid, self-organizes into spatiotemporally periodic patterns. In this paper, we wish to address this issue by studying vortex shedding and street formation using rods of different geometric cross-sectional areas but with their aspect ratios close to unity. The experiment is conducted in freely flowing soap films that strongly suppresses instabilities and turbulence, which are commonly encountered in three dimensional (3D) fluids when Reynolds number Re is large. Our quasi 2D experiments therefore allow *laminar vortex streets* to be studied over a broad range of Re .

In an earlier paper, we showed that a $St - Re$ relation can be derived based on simple observations of vortex streets beneath a circular rod [6]. Specifically, if the flow speed U is held constant and Re is varied by changing the diameter D of the rod, the experiment shows that the wavelength of the vortex street λ is a linear function of D , $\lambda = \lambda_0 + \alpha D$, that spans the entire range of Re ($10 - 3 \times 10^3$) in the measurement, where $\lambda_0 \simeq 0.1$ cm and $\alpha \simeq 4$ are constant. Another simplifying feature observed in the experiment is that over the same span of Re , vortex street travels at a constant speed v_{st} relative to the background flow U so that $c(\equiv v_{st}/U) \simeq 0.8$ remains constant for different D . Since the laminar vortex street represents a single global mode of fluid dynamics, its frequency must satisfy $f = v_{st}/\lambda$. Using the definition of $St(\equiv fD/U)$, it follows immediately that $St = 1/(A + B/Re)$, or more concisely

$$\frac{1}{St} = A + B \cdot \frac{1}{Re}, \quad (1)$$

where $A = \alpha/c$ and $B = \lambda_0 U/(c\nu)$ are constant.

Eq. (1) works well for measurements using circular rods in 3D fluids as well as in 2D soap films as discussed in Ref. [6]. Unlike previously proposed $St - Re$ relation that is either applicable to vortex streets near an onset [7–9] or very far from it [3], the remarkable fact is that Eq. (1) is applicable to both low and high Re . The robustness of this relationship is a testament of the fact that our empirical approach is capable of capturing important features of vortex street behind a bluff body. The purpose of the current research is therefore two folds: (i) to further explore this approach by investigating vortex streets created by (blunt) bodies of different shapes, and (ii) how the shape affects the wake parameters, such as α , λ_0

and c , and ultimately the $St - Re$ relationship. Aside from its scientific interest, the inquiry is useful to a variety of engineering problems where vortex shedding and wake formation play an important role.

Our experiment was carried out in an inclined soap-film channel depicted in Fig. 1(a) [10, 11]. The soap solution consisted of 2% Dawn detergent, 5% glycerol, and water, giving a bulk kinematic viscosity $\nu \simeq 0.013 \text{ cm}^2/\text{s}$. The film was 2 m long, 5 cm wide, and flowed continuously with a mean speed $U \simeq 60 \pm 3 \text{ cm/s}$. At this speed, the film has a thickness $\sim 3 \mu\text{m}$ as determined by a laser transmission method and is weakly compressible with a Mach number $Ma \simeq 0.12$ [12]. Our flowing soap film therefore served as a quasi-2D fluid medium with its slight compressibility facilitating instantaneous flow visualization using a low-pressure sodium lamp and a high-speed video camera. In this regard, the use of a soap film is very attractive because the boundary layer separation can be readily visualized without using dyes or other agents. The physical basis of such flow visualization is that for a weakly compressibility fluid, such as a soap film, the conserved quantity is ω/ρ_2 , where ω is the vorticity and $\rho_2 = \rho h$ is the 2D density of the film. The variation of ω is thus accompanied by a variation in h , since the water density ρ is constant. The technique is also very sensitive because the film thickness variation Δh is measured in terms of wavelength of the sodium lamp (589 nm); a mere change of $\lambda/4$ in the thickness will cause a change from constructive (bright) to destructive (dark) interference in our video images. As Figs. 1(b,c) illustrate, the technique allows direct measurements of flow structures, such as the wavelength λ and the street width h , and dynamic parameters, such as U , v_{st} , and f . These measurements were made without post processing of images. Here the shedding frequency f was determined by two methods: (i) directly counting the number of vortices shed per second, and (ii) using the ratio v_{st}/λ at a fixed downstream distance y . Both methods yields essentially the same result as in Ref. [6].

Vortex streets were created using tapered rods of different geometrical cross sections, circle (C), square (S), diamond (D), and equilateral triangle (T), as depicted in Fig. 3(a-d). A circular rod was made of glass using a glass puller. All other rods, including another circular one, were made of titanium carefully machined to have the tip size $\lesssim 50 \mu\text{m}$; the small tips allow vortex street to be studied at small Re . Two circular rods, made of glass and titanium, give identical results, suggesting that the surface chemistry may not play a crucial role (also see Fig. 4.3(e) of Ref. [13]). To significantly reduce run-to-run variations,

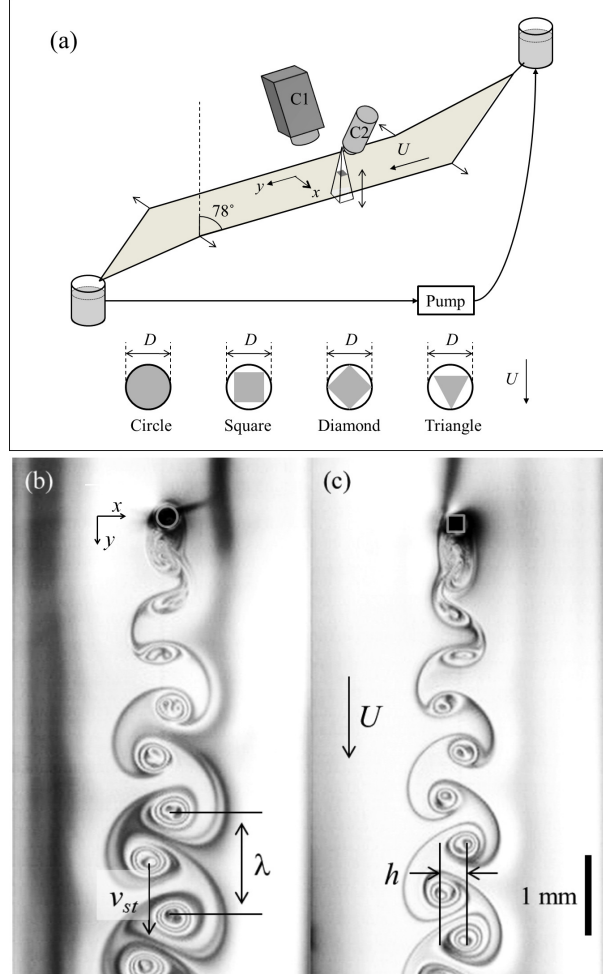


Figure 1. (a) Experimental Setup. The soap film channel is inclined at 12° from horizontal. A fast video camera C1 (Vision Research, Phantom V5) and a microscope C2 (Wild M5A) equipped with a CMOS camera (DCM130, Oplenic) are mounted directly above the film. Four different shaped rods, circular (C), square (S), diamond (D), and triangular (T), are used for measurements, and their characteristic size are defined as D . Panels (b) and (c) display the vortex streets created by a circular and a square rod, respectively. The Reynolds number, $Re \simeq 170$, is about the same for both cases.

we maintained a constant film thickness by keeping the flow speed U fixed. As delineated in Fig. 1(a), $Re(\equiv UD/\nu)$ can be varied by changing the size D of the rod using a translation, and D is measured by a CMOS camera mounted on a long-working distance microscope.

As depicted in Figs. 1 (b-c), directly beneath the rods, vortices detach periodically from the rod, they then undergo a transient relaxation over a downstream distance y , and finally

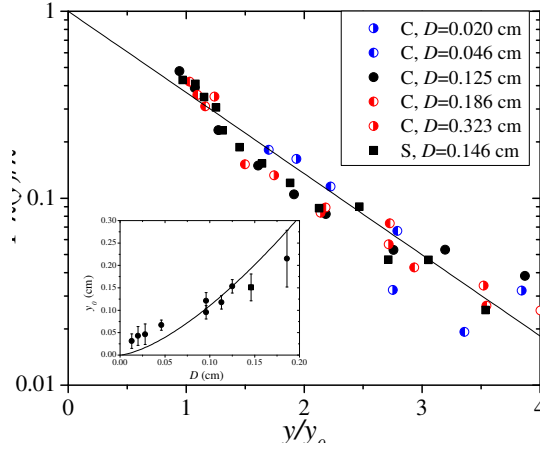


Figure 2. (Color online) The downstream-distance dependent Wavelength $\lambda(y)$ vs. y . For all different rods, For circular (C) and square (S) rods, the wavelength of their vortex streets depend on the downstream distance y and can be accurately described by $\lambda(y) = \lambda(1 - e^{-y/y_0})$, which is shown by the solid line. The inset shows that the decay length y_0 depends on the size of the rods, D , and scales approximately as $D^{3/2}$ as delineated by the solid line. This scaling behavior is predicted by Eq. (6).

organize into a steady-state confirmation. The wavelength $\lambda(y)$ of a vortex streets therefore depends on y , and reaches a constant value λ for $y \gtrsim 10D$. When $1 - \lambda(y)/\lambda$ is plotted against y , as depicted in Fig. 2 for C and S rods, all the data for different D follows a linear behavior, suggesting an exponential dependence,

$$\lambda(y) = \lambda \left(1 - e^{-y/y_0} \right), \quad (2)$$

where y_0 is the decay length. Systematic measurements, such as this one, were carried out for the four rods, C, S, D, and T, and their steady-state wavelengths λ as a function of D are displayed in Figs. 3 (a-d). For all the cases we found that λ , to a good degree, depends on D linearly, and the results of fitting using $\lambda = \lambda_0 + \alpha D$ are delineated by the red lines in the figures. Our experiment shows that the intercepts λ_0 vary from rod to rod, but they are all very small about a millimeter or so (see Table I). The slope α also depend on the shape of the rods with the largest $\alpha = 4.3 \pm 0.1$ for the C rod and the smallest $\alpha = 3.1 \pm 0.1$ for the T rod.

In Figs. 3(e-h), velocity of vortex streets relative to the mean flow, v_{st}/U , is plotted as a

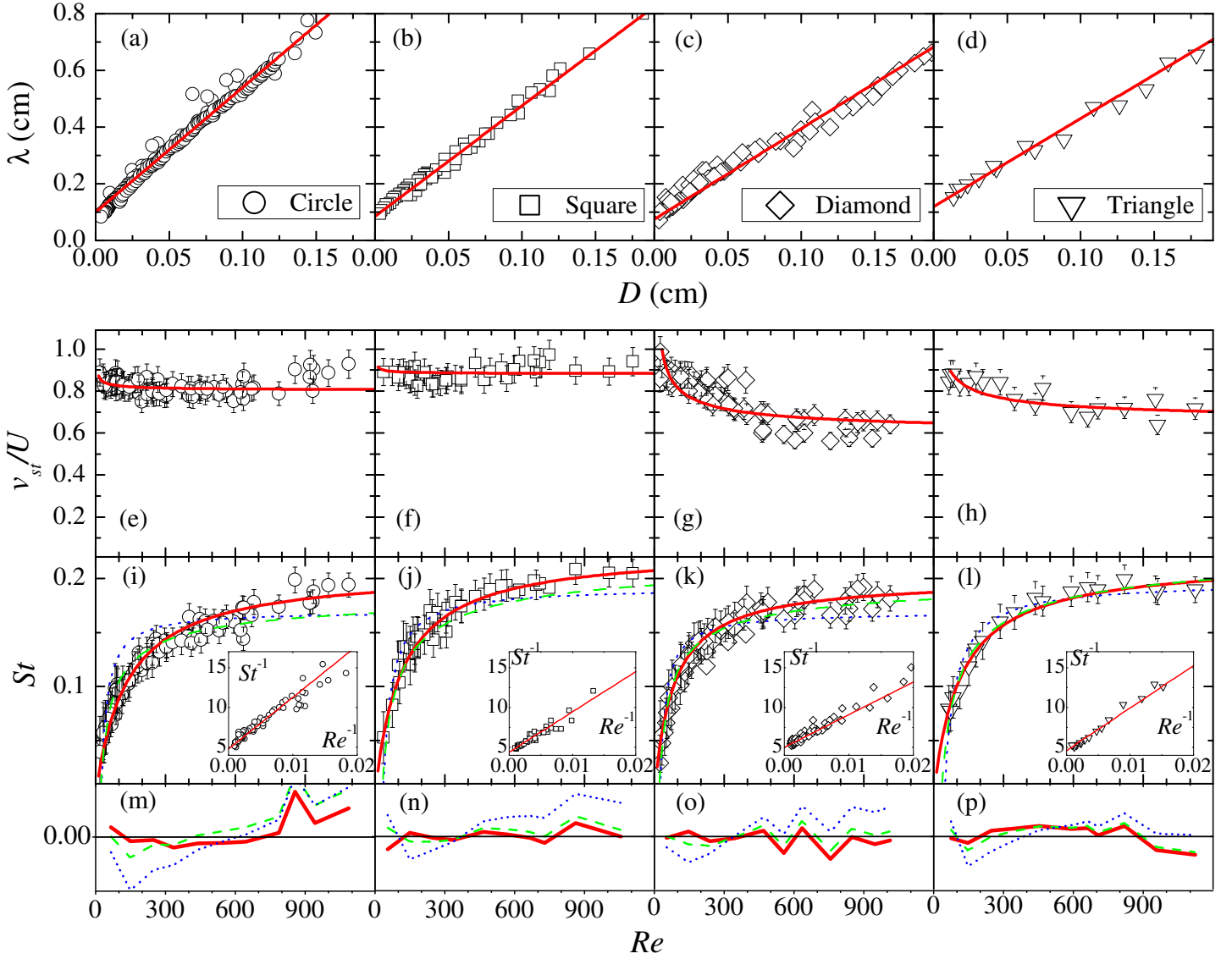


Figure 3. (Color online) Experimental Results. The top panels (a-d) display λ vs. D for circular (C), square (S), diamond (D), and triangular (T) rods, respectively. In all the cases, λ varies linearly with D but with a finite intercept λ_0 that varies little among different rods. The middle panels (e-h) are v_{st}/U vs. Re for the same set of rods. For C and S rods, v_{st}/U is approximately constant throughout the whole range of Re . However, for D and T rods, v_{st}/U decreases monotonically with Re and eventually reaches a plateau value defined as c . The bottom panels (i-l) display St vs. Re for the four rods. The red solid line, green dash line, and blue dotted lines in (i-l) are fitting curves using respectively Eq. (1), $St = a' - b'/\sqrt{Re}$ [14, 15], and the classical relation $St = a(1 - b/Re)$. The corresponding residuals of the fits are shown in (m-p). In the insets of (i-l), the same graphs are replotted using St^{-1} vs. Re^{-1} . The linear relation suggests the validity of Eq. (1), and moreover the intercepts, $St_{\infty}^{-1} \simeq 4.6$, are about the same for all the rods.

function of Re . Physically, the speed v_{st} by which a vortex street travels in the background flow U depends on the vortex strength κ . Since κ is small near the onset, one expects $v_{st}/U \rightarrow 1$, i.e. vortices are passively convected by the mean flow. However, as Re increases and circulation in vortices becomes larger, one expects v_{st}/U to decrease. This qualitative behavior is indeed observed for D and T, where v_{st}/U decays monotonically as Re increases and levels off $v_{st}/U \rightarrow c$ for $Re > 400$. Curiously, this behavior is absent for C and S rods, where v_{st}/U is nearly constant for the whole range of Re ; the quantity v_{st}/U may even increase slightly with Re , which results from mixing of vorticity of opposite signs at very large Re . The plateau value c is found to depend on the shape of rods as detailed in Table with $c \simeq 0.81, 0.86, 0.63$, and 0.70 for C, S, D, and T, respectively. The small c values for D and T rods suggest that vorticity κ is more efficiently encapsulated into vortices by the rods with a trailing edge than rods without it. Since in our experiment, the mean flow U is fixed, the above findings cannot be a result of air damping. The effect can be understood, however, by the fact that a trailing edge reduces the base suction pressure and keeps the two separated boundary layers physically apart, reducing their mixing. This results in a wider wake or a larger Kármán ratio, $K_r \equiv h/\lambda$, as will be discussed later.

It is useful at this point to compare our measurements with von Kármán's point vortex model that makes predictions about the speed ratio of the vortex street: $v_{st}/U = 1 - (\kappa/2U\lambda) \tanh(\pi h/\lambda)$ [3]. Assuming that Kármán's stability condition [16], $\tanh(\frac{h\pi}{\lambda}) = 1/\sqrt{2}$, holds in the experiment and vorticity created in the boundary layer is 100% encapsulated into the eyes of vortices, $\kappa = \lambda U$ [17], we found $v_{st}/U = 1 - \frac{1}{2\sqrt{2}} \simeq 0.65$. This value is remarkably close to the plateau value c measured for D and T rods, suggesting that these geometries permit nearly maximum preservation of vorticity in the wake region. It also suggests that when Re is not large or when objects do not have a trailing edge, such as C or S rod, a noticeable amount of vorticity is annihilated before a stable vortex street is formed.

We now turn our attention to the St - Re relation for different rods. Here, the frequency f was determined by counting the number N of vortices shed per second ($f = N/2$) and then non-dimensionalized to obtain the Strouhal number, $St = fD/U$. We found that in all cases laminar vortex streets persist over a wide range of Re , $10 < Re < 1200$, which is in a sharp contrast with 3D measurements [18–20]. As delineated in Figs. 3(i-l), different rods exhibit similar St - Re dependence, i.e. St increases rapidly for small Re and levels off for large Re . These behaviors can be accurately captured by Eq. (1) as delineated by the

	C	S	D	T
c	0.81 ± 0.04	0.86 ± 0.05	0.63 ± 0.05	0.71 ± 0.07
α	4.3 ± 0.1	3.9 ± 0.1	3.2 ± 0.1	3.1 ± 0.1
λ_0 (mm)	1.00 ± 0.03	0.85 ± 0.06	0.75 ± 0.04	1.2 ± 0.1
A	5.1 ± 0.2	4.4 ± 0.2	5.0 ± 0.2	4.6 ± 0.2
B	580 ± 32	468 ± 25	456 ± 29	549 ± 44
α/c	5.3 ± 0.3	4.5 ± 0.4	5.1 ± 0.5	4.4 ± 0.6
$\lambda_0 U/c\nu$	577 ± 77	456 ± 81	549 ± 104	791 ± 200

Table I. Measured Wake Parameters. For each shape (circle (C), square (S), diamond (D), and triangle (T)) of the rod, parameters c , α and λ_0 are determined from Figs. 3(a-h). Coefficients A and B are determined using the plots in the insets of Figs. 3(i-l). For comparison, α/c and $\lambda_0 U/c\nu$ are also tabulated, and they provide an alternative means to obtain A and B coefficients.

solid red lines in the figures. The appropriateness of Eq. (1) is further checked by plotting St^{-1} vs. Re^{-1} as displayed in the inset, where indeed good linear relationships are found. The A and B coefficients extracted from these plots are listed in Table I, and overall they compare quite well with those calculated based on structural measurements using $A \equiv \alpha/c$ and $B \equiv \lambda_0 U/c\nu$. The largest discrepancy of $\sim 30\%$ is for coefficient B of D and T rods, and it is due to approximating v_{st}/U by a constant c , which according to Figs. 3(c) and (d) is valid only for large Re . Surprisingly, even in these cases, parametrization of $St - Re$ relation using only two parameters (A and B) appears to be adequate based on linearity of the data in the insets of Figs. (k-l). The most noteworthy feature of these measurements is the fact that asymptotically ($Re \gg 1$) the Strouhal number $St_\infty \simeq 0.21 \pm 0.02$ turns out to be nearly the same for different rods. This suggests that St_∞ (or A) is a property of the downstream wake rather than properties of the obstacle that creates it. In Ref. [8], it has been proposed that street formation is a global instability of the wake, and our measurement is consistent with this physical picture. Our finding furthermore suggests that for blunt bodies, the mode selection in the high Re regime is independent of the body shape, indicating that this mode may be universal.

Inspection of a vortex street near a rod reveals a streak of fluid that oscillates periodically in a fashion similar to a physical pendulum (see Fig. 4). This observation was exploited by

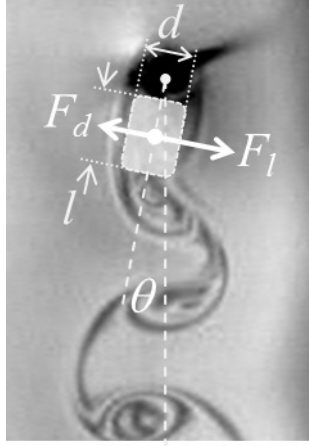


Figure 4. The Free-Body Diagram Representing Birkhoff's Pendulum Model. Swing of a fluid element in the near wake region is approximated by a physical pendulum of length ℓ and width d as indicated. The restoring force is the lift indicated by F_l and the damping force is indicated by F_d .

Birkhoff to explain the experimentally observed $St-Re$ relationship when $Re \gg 1$ [3]. Below we generalize Birkhoff's simple model to include viscous damping. As we shall see that with such a modification, certain features of vortex streets observed in our experiment can be described. For a lamina inclined at an angle θ to the stream, it is well-known that the lift coefficient is $C_L = 2\pi\theta$ [21]. This gives the cross-force per unit length $F_l = \frac{1}{2}\rho U^2 C_L = \pi\rho U^2\theta$. For the fluid element of width d and length ℓ behind the rod, the inertia force per length is $\rho d(\ell\ddot{\theta})$, where ρ is the 2D density. As for the damping term, the drag force per unit length is $F_d = \frac{1}{2}\rho U^2 C_D$, where C_D is the drag coefficient. For a cylinder, measurements showed $C_D \propto 1/\sqrt{Re}$ over a broad range of Re , $10 \leq Re \leq 10^3$ [22]. It follows from a simple dimensional analysis that the damping force per length is $\gamma_0\rho\nu\sqrt{Re'}\dot{\theta}$, where $Re' = U\ell/\nu$ and γ_0 is a dimensionless constant characterizing the overall magnitude of damping. Balancing these forces yields,

$$\ddot{\theta} + 2\tau_0^{-1}\dot{\theta} + \omega_0^2\theta = 0. \quad (3)$$

This equation describes the damped harmonic oscillations with a decay time $\tau_0 = 2d\ell/\gamma_0\nu\sqrt{Re'}$ and a natural frequency $\omega_0 = U\sqrt{\pi/d\ell}$. If one assumes $\theta = \theta_0 \exp(\Lambda t)$, the characteristic

value Λ is given by,

$$\Lambda = -\tau_0^{-1} \pm i\sqrt{\omega_0^2 - \tau_0^{-2}}. \quad (4)$$

Since the width of the wake is approximately the size D of a rod, we make an ansatz $d = D$ and $\ell = kD$, where k is a phenomenological parameter [3]. It follows from Eq. (4) that the oscillation frequency f of the wake is given by,

$$\begin{aligned} f &= \frac{\text{Im}(\Lambda)}{2\pi} = \frac{U}{2\sqrt{\pi d \ell}} \left(1 - \frac{\gamma_0^2 \nu}{4\pi U d}\right)^{1/2} \\ &\simeq \frac{U}{2D\sqrt{k\pi}} \left(1 - \frac{\gamma_0^2}{4\pi Re}\right)^{1/2}, \end{aligned} \quad (5)$$

where $Re \equiv UD/\nu$. In the small-damping limit ($\gamma_0^2/(4\pi Re) \ll 1$), Eq. (5) gives $St^{-1}(\equiv U/fD) = St_\infty^{-1}(1 + \gamma_0^2/8\pi Re)$, which has the same mathematical form as the phenomenologically derived $St-Re$ relation, Eq. (1). Here $St_\infty \equiv 1/2\sqrt{k\pi}$ is the asymptotic Strouhal number and is identical to Birkhoff's result [3]. Since $St_\infty \simeq 0.2$ is nearly a constant for different rods (see Fig. 3(i-l)), it may be concluded that $k = 2$ and $St_\infty = 1/2\sqrt{2\pi}$ is universal for a laminar vortex wake. We also notice that in the same small-damping limit, Eq. (5) yields the experimentally observed linear D dependence for λ , $\lambda = \lambda_0 + \alpha D$, where $\alpha = 2\sqrt{2\pi}c$ and $\lambda_0 = c\gamma_0^2\nu/2\sqrt{2\pi}U$. For a circular rod and using $c = 0.81$ in Table I, we found $\alpha \simeq 4.1$, which is in reasonable agreement with the slope $\alpha \simeq 4.3$ seen in Fig. 3(e).

Finally, the real part of Eq. (4) gives the characteristic relaxation time τ_0 of the oscillation,

$$\tau_0 = \frac{1}{\text{Re}(\Lambda)} = \frac{2\sqrt{kRe}}{\gamma_0} \frac{D}{U}. \quad (6)$$

If one associates τ_0 with the decay length y_0 of the wake defined in Eq. (2)), i.e. $y_0 \simeq v_{st}\tau_0$, Eq. (6) suggests the scaling $y_0 \propto D^{3/2}$. In the inset of Fig. 2, this predicted relationship (solid line) is compared with the measured decay length y_0 vs. D for C rod. The agreement is fair considering that uncertainties in the measurement is quite large.

In summary, we showed that the phenomenologically derived $St-Re$ relation, Eq. (1), is applicable to vortex shedding behind blunt bodies other than circular ones. Specifically, the A and B coefficients in the equation are determined respectively by two characteristic length scales D and λ_0 in the flow. A significant finding of this work is that in the high Re regime, the wake oscillation frequency f is uniquely determined by the largest length scale D in the problem, resulting in $St_\infty \rightarrow 1/A \simeq 0.21$ (or $f \simeq 0.21U/D$) for all different rods. On the

other hand, in the low and intermediate Re regimes, where the fluid viscosity cannot be neglected, λ_0 also contributes to vortex shedding, and St becomes shape dependent. There exists a strong correlation between the street velocity v_{st} , characterized by $c = v_{st}/U$ at large Re , and the shape of a body, e.g., for bodies with a trailing edge, such as D and T rods, c are significantly lower than that of C and S rods. Since c is a measure of the vortex strength κ , it can be concluded that the trailing edge allows more powerful vortices to be shed and better preserved downstream. We noticed moreover that when c is small, the wake parameter α is also small. This gives rise to interesting properties of a wake, such as $St_\infty = 1/A \simeq c/\alpha$ being weakly shape dependent but the Kármán ratio $K_r = h/\lambda$ strongly shape dependent. The latter can be seen by noticing that since $h \simeq D$ and $\lambda = \lambda_0 + \alpha D \simeq \alpha D$, the Kármán ratio is given by $K_r \simeq \alpha^{-1}$. For C, S, D, T rods, we obtained $K_r \simeq 0.23, 0.25, 0.31$, and 0.32 , respectively. In Kármán's classical calculation, it was found that point vortex street is stable when $K_r = \frac{1}{\pi} \cosh^{-1} \sqrt{2} \simeq 0.28$. Our experiment shows that vortex streets generated with different shaped rods have K_r not exactly as Kármán had predicted, but interestingly they all appear to be stable.

This work is supported by the NSF under the grant no. DMR-0242284.

-
- [1] V. Strouhal, Ann. Physik **5**, 216 (1878).
 - [2] L. Rayleigh, Philos. Mag. **29**, 433 (1915).
 - [3] G. Birkhoff, J. Appl. Phys. **24**, 98 (1953).
 - [4] A. Roshko, NACA Report **No. 1191** (1954).
 - [5] C. H. K. Williamson, Ann. Rev. Fluid Mech. **48**, 477 (1996).
 - [6] P. Roushan and X. L. Wu, Phys. Rev. Lett. **94**, 054504 (2005).
 - [7] M. Provansal, C. Mathis, and L. Boyer, J. Fluid. Mech. **182**, 1 (1987).
 - [8] P. Monkewitz, Phys. Fluids **51**, 999 (1988).
 - [9] J. Chomaz, P. Huerre, and L. Redekopp, Phys. Rev. Lett. **60**, 25 (1988).
 - [10] X. L. Wu, R. Levine, M. Rutgers, H. Kellay, and W. I. Goldburg, Rev. Sci. Instrum. **72**, 3025 (2001).
 - [11] D. Georgiev and P. Vorobieff, Rev. Sci. Instrum. **73**, 1177 (2002).
 - [12] I. Kim and X. L. Wu, Phys. Rev. E **82**, 026313 (2010).

- [13] T. A. Tran, *Experiments in turbulent soap-film flows: Marangoni shocks, frictional drag, and energy spectra*, Ph.D. thesis, University of Illinois (2011).
- [14] U. Fey, M. König, and H. Eckelmann, Phys. Fluids **10**, 1547 (1998).
- [15] C. H. K. Williamson and G. L. Brown, J. Fluids Struct. **12**, 1073 (1998).
- [16] T. von Kármán, Gottinger Nachr , p.509 (1911).
- [17] J. Synge, Proc. Roy. Irish Acad. **37**, 95 (1927).
- [18] C. H. K. Williamson, Phys. Fluids **31**, 3165 (1988).
- [19] C. Norberg, J. Fluid. Mech. **258**, 287 (1994).
- [20] H.-Q. Zhang, U. Fey, B. R. Noack, M. König, and H. Eckelmann, Phys. Fluids **7**, 779 (1994).
- [21] L. Landau and E. Lifshitz, *Fluid Mechanics*.
- [22] H. Schlichting, *Boundary-Layer Theory*.